PAPER • OPEN ACCESS

Simulations of paraffine melting inside metal foams at different gravity levels with preliminary experimental validation

View the article online for updates and enhancements.

IOP ebooks™

Bringing together innovative digital publishing with leading authors from the global scientific community.

Start exploring the collection−download the first chapter of every title for free.

Simulations of paraffine melting inside metal foams at different gravity levels with preliminary experimental validation

M Iasiello[*,#]**, M Mameli**[**]**, S Filippeschi**[**] **and N Bianco**[*]

* Dipartimento di Ingegneria Industriale - Università degli Studi di Napoli Federico II - Piazzale Tecchio, 80 - 80125 – Napoli – Italy

** Dipartimento dell'Energia dei Sistemi del Territorio e delle Costruzioni - Università di Pisa – Largo Lazzarino, 2 - 56121 – Pisa – Italy

[#] Email: marcello.iasiello@unina.it

Abstract. In this work, the results of a numerical code based on the porous media Local Thermal Non-Equilibrium (LTNE) and the apparent heat capacity methods, are compared with experiments aiming at a preliminary validation. The test cell consists in a 50 mm aluminum foam cube filled with a paraffin wax, heated and cooled on the same face. The heat flux is measured by two miniaturized sensors, while the temperature is measured in three different locations along the cube edge. Finally, one side is equipped with a Zinc Selenide window which is transparent to the long wave InfraRed. This system allows to track the paraffin melting front evolution together with the temporal trend of the whole temperature distribution simplifying the comparison with the numerical outputs at different time steps.

The numerical model is then set with the same boundary conditions (heat flux) to predict the experimental temperature fields, considering both conduction in the solid domain and natural convection in the liquid domain. The preliminary validation shows that the numerical results match the experimental data with good agreement. Results are also presented for different gravity levels. This study can be a starting point for all those applications where gravity has a major role.

Nomenclature

A_{mush}	Volume force constant (kg/m³ s)		T	Temperature (K)
C_F	Inertial factor		$/\mathbf{u}/$	Velocity vector (m/s)
C_p	Heat capacity (J/kg K)			
d_c	Cell size (m)		**Greek symbols**	
d_s	Strut size (m)		α	Isobaric compressibility (1/K)
$\mathbf{g}$	Gravity acceleration (m/s²)		β	Melting fraction function
G	Geometric function		ε	Porosity
h_c	Interfacial heat transfer coefficient (W/m² K)		λ	Latent heat of fusion (J/kg K)
h_v	Volumetric heat transfer coefficient (W/m³ K)		μ	Viscosity (Pa s)
k	Thermal conductivity (W/m K)		ρ	Density (kg/m³)
K	Permeability (m²)			
Nu_s	Strut Nusselt number		**Subscripts**	
p	Pressure (Pa)		d	Dispersion
Pr	Prandtl number		eff	Effective
$/\mathbf{q}/$	Heat flux (W/m²)		m	Melting
q_{mush}	Volume force constant		PCM	Phase Change Material

Ra_s	Strut Rayleigh number		s	Solid foam
S	Volume force term (kg/m^3 s)			
S_v	Specific surface area (1/m)		**Superscripts**	
t	Time (s)		*PCM*	Phase Change Material
			s	Solid foam

1. Introduction

Thermal energy storage systems are very important to achieve large amounts of heat, especially for renewable energies, in which the font availability might be an issue [1-3]. In particular, latent storage systems are promising since they can store large amounts of heat with low temperature differences. Among various latent storage systems, Phase Change Materials (PCMs) seem to be one of the most promising in terms of efficiency and cost ratio. Depending on the desired application, the PCMs can be chosen based on melting/solidification temperatures. Despite their capability to store large amounts of heat, they present a low thermal conductivity that needs to be enhanced to melt the whole volume in reasonable times. Various techniques have been proposed during the years, like nanoparticles, expanded graphite, encapsulation or metallic foams [4]. In particular, metallic foams based on highly conductive materials like aluminum or copper are promising since they consist into a sponge-like material that is filled with the phase change material, so that the overall thermal conductivity and melting times are respectively increased and reduced. Wang et al. [5] showed that the equivalent thermal conductivity of a paraffin/copper foam can be 50 times the paraffin thermal conductivity.

Several experimental and numerical studies have been presented through the years about combining metallic foams with PCMs. Experiments have been carried out by Mancin et al. [6] on three paraffin with different melting points and heat fluxes, by employing foams with different pore densities (PPIs) at equal porosity. They showed that foams increase the heat transfer capability of phase change materials, achieving lower temperatures, and that no relevant effects are referred to foams with different PPIs. Aluminum foams have been investigated by Lafdi et al. [7]. They analyzed foams with different PPIs and porosity, showing that foams with higher porosity and lower PPIs permit to achieve steady state faster than lower porosity and higher PPIs foams because of convection effects. On the other hand, they also conclude that temperatures are generally lower for lower porosity foams because of the higher overall thermal conduction.

Numerical studies have been proposed during the years. First of all, the three-phases media can be modeled by using the porous media theory [8], in which governing equations for PCM and foams are averaged over a representative elementary volume. Energy equations can be modeled either considering the Local Thermal Equilibrium (LTE), in which both components are in local thermal equilibrium [9], or with a Local Thermal Non Equilibrium (LTNE) model, in which the heat exchange between the two phases is taken into account via a volumetric heat transfer coefficient [10, 11]. The PCM phase change can be modeled by employing the enthalpy method, as in Tian and Zhao [12], or the apparent heat capacity method, in which it is assumed that the heat capacity during phase change is not infinite but it achieves a very high value that depends on latent heat of solidification, as in Li et al [13].

During the years it has been shown in many studies that natural convection inside PCMs may have a role depending on the entity of the buoyancy forces, and in some conditions it cannot be neglected to achieve good predictions. An example of PCM applications in such conditions can be a closed-loop pulsating heat pipe for a sounding rocket [14], in which a phase change material is used as the heat pipe condenser. In this study, numerical results are presented under different gravity conditions for a paraffin wax embedded into a 40 PPI aluminum foam with nominal porosity of 0.88. Numerical model is built up based on LTNE and apparent capacity methods and solved with finite element method, and comparisons with experiments run at normal gravity level are also presented.

2. Numerical modeling

The investigated PCM is a paraffin whose properties are reported in Table 1. Metal foam herein investigated is an aluminum foam manufactured by ERG Aerospace with nominal porosity of 0.88 and 40 PPIs. Aluminum thermal conductivity, density and heat capacity are respectively 220 W/m K, 2700 kg/m^3 and 900 J/kg K. The experimental setup of the PCM/foam is described in detail in the experiments section afterwards. Because it is assumed that all the walls of the PCM/foam are adiabatic except the one that faces Peltier cell, the geometrical model for the prediction is a 2D square with a 0.05 m side.

Governing equations are written with references to porous media theory and by assuming local thermal non-equilibrium between the two phases. For each REV of the two components (PCM and aluminum foam), mass, momentum and energy equations are written under the assumptions of incompressible laminar flow and Boussinesq assumption

$$\frac{\partial \rho_{PCM}}{\partial t} + \nabla \cdot \left(\rho_{PCM} \langle \mathbf{u} \rangle \right) = 0 \tag{1}$$

$$\frac{\rho_{PCM}}{\varepsilon \beta} \frac{\partial \langle \mathbf{u} \rangle}{\partial t} + \frac{\rho_{PCM}}{(\varepsilon \beta)^2} \left(\langle \mathbf{u} \rangle \cdot \nabla \langle \mathbf{u} \rangle \right) = -\nabla \langle p \rangle + \frac{\mu_{PCM}}{\varepsilon \beta} \nabla^2 \langle \mathbf{u} \rangle - \frac{\mu_{PCM}}{K} \langle \mathbf{u} \rangle - \frac{\rho_{PCM} C_F}{\sqrt{K}} |\langle \mathbf{u} \rangle| \langle \mathbf{u} \rangle +$$
$$+ \rho_{PCM} \mathbf{g} \alpha \left[\langle T_{PCM} \rangle^{PCM} - \left(T_m - \Delta T_m \right) \right] - S \left(\langle T_{PCM} \rangle^{PCM} \right) \langle \mathbf{u} \rangle \tag{2}$$

$$\varepsilon \left(\rho C_p \right)_{PCM} \left(\frac{\partial \langle T_{PCM} \rangle^{PCM}}{\partial t} + \langle \mathbf{u} \rangle \cdot \nabla \langle T_{PCM} \rangle^{PCM} \right) = \nabla \cdot \left(k_{eff,PCM} \nabla \langle T_{PCM} \rangle^{PCM} \right) +$$
$$+ h_v \left(\langle T_s \rangle^s - \langle T_{PCM} \rangle^{PCM} \right) - \varepsilon \rho_{PCM} \lambda \frac{\partial \beta}{\partial t} \tag{3}$$

$$\left(1 - \varepsilon \right) \left(\rho C_p \right)_s \frac{\partial \langle T_s \rangle^s}{\partial t} = \nabla \cdot \left(k_{eff,s} \nabla \langle T_s \rangle^s \right) - h_v \left(\langle T_s \rangle^s - \langle T_{PCM} \rangle^{PCM} \right) \tag{4}$$

In the momentum equation, the source term is employed in order to force solution to zero when PCM becomes solid

$$S \left(\langle T_{PCM} \rangle^{PCM} \right) = A_{mush} \frac{\left(1 - \beta \right)^2}{q_{mush} + \beta^3} \tag{5}$$

Where the constant q_{mush} is equal to 10^{-3} to avoid division by zero, while A_{mush} is equal to 10^4, that is a good compromise between computational effort and solution accuracy [19]. Besides, the function β is an interpolation function that is 10^{-6} to avoid division by zero in equation (2) when PCM temperature is below T_m-ΔT, and 1 if the temperature is higher than T_m+ΔT; the function is also smoothed in the transition points in order to guarantee that second derivative is continuous everywhere.

In order to close equations (1) – (4), closing coefficients for porous media are required. These are reported in the following, together with reference number. Boundary conditions of the problem are listed in the following. For the momentum equation, it is assumed that the velocity is zero everywhere. For the energy equations, adiabatic conditions are invoked everywhere, except for the Peltier cell face. In particular, for the solid phase equation, entering heat flux is equal to 11520 W/m^2; on the other hand, for the fluid phase equation it is assumed that both phases are in thermal equilibrium, *i. e.* $<T_{PCM}>^{PCM} = <T_s>^s$. It has been shown from preliminary simulations that thermal dispersion due to convection doesn't have any relevant effect on a qualitatively evaluation of both melting front evolution and melting fraction.

Table 1. PCM thermophysical properties and porous media coefficients.

Parameter	Value	Coeff.	Equation	Ref.
			$$K = 0.00073(1-\varepsilon)^{-0.224}\left(\frac{d_s}{d_c}\right)^{-1.11}$$	[15]
ρ_{PCM}	850 kg/m³	K	$$d_c = \left[-0.921\ln(PPI)+5.3564\right]10^{-3}$$	[20]
			$$\frac{d_s}{d_c} = \frac{1.18}{G}\sqrt{\frac{1-\varepsilon}{3\pi}}$$	[15]
			$$G = 1 - e^{\left[-(1-\varepsilon)/0.04\right]}$$	[15]
μ_{PCM}	3.85 mPa s	C_F	$$C_F = 0.00212(1-\varepsilon)^{-0.132}\left(\frac{d_s}{d_c}\right)^{-1.63}$$	[15]
			$$h_v = h_c S_v = \mathrm{Nu}_s \frac{k_{PCM}}{d_s} S_v$$	
α	7.78·10⁻⁴ 1/K	h_v	$$\mathrm{Nu}_s = 0.36 + 0.521\left\{\frac{\mathrm{Ra}_s}{\left[1+(0.442/\mathrm{Pr})^{9/16}\right]^{16/9}}\right\}^{1/4}$$	[16]
			$$\mathrm{Ra}_s = \rho_{PCM}^2\, \mathbf{g}\beta|\mathbf{q}|d_s^4 \big/ \left(k^2\mu C_p\right)_{PCM}$$	
			$$S_v = \frac{G}{0.59}\frac{3\pi d_s}{d_c^2}$$	[15]
T_m	330 K	$k_{eff,PCM}$	$$k_{eff,PCM} = \varepsilon k_{PCM} + k_d$$ $$k_d = \frac{0.36}{1-\varepsilon}\left(\rho C_p\right)_{PCM} d_s|\mathbf{u}|$$	[17]
ΔT_m	1 K	$k_{eff,s}$	$$k_{eff,s} = 0.316(1-\varepsilon)k_s$$	[18]
$C_{p,PCM}$	2490 J/kg K			
k_{PCM}	0.2 W/m K			
λ	185 kJ/kg K			

Equations are solved with the finite element commercial code COMSOL Multiphysics. Streamline and crosswind stabilization are used for PCM mass and momentum equations. A free time step with a maximum of 60 s is used for the time-variable discretization, while a 100x100 square elements grid is used. Convergence criterion of 10^{-3} for each time step herein simulated is used.

3. Experiments

A sketch of the experimental test cell is shown in figure 1. The test section with aluminium foam and the paraffin wax is a 50x50x50 ± 0.5 mm cube. The aluminum foam is filled with liquid paraffin wax (filling ratio 95-97% of the free volume) and located in a Lexan box which provides a thermal insulation from the environment and that allows the visualization of melting and solidification process with a CMOS camera (2048 x 2048 pixel, 12-bit RGB). A window of the cubic box is made of Zinc Selenide (ZnSe) to record the evolution of temperatures and the front melting/solidification by means of a Low Wave Infrared Camera (LWIR) FLIR® A65. The aluminium foam surface facing the IR window as well as the Pt-100 sensor visible by the IR camera have been black painted (emissivity > 0.95) to avoid reflection issues. An external Aluminum box contains the polycarbonate box and it is designed to withstand the LDC accelerations and the internal pressures originated by the melting of the paraffin wax.

The test cell consists of the heating/cooling system, the composite material and the containing box. The first is a Peltier module (40x40x5 mm) connected with on one side with the the aluminum plate where the foam is brazed and on the other side to an active cooling system by means of a high thermal conductive paste. Besides, the experimental apparatus is equipped also with two heat flux sensors, 4 Pt-100 sensors, the Main Control Unit (MCU), the Power Control Unit (PCU) of the Peltier cell, a Data Acquisition Unit (DAU), a video camera and a IR camera. The system allows to monitor the state of the experiment box and peripherals, to drive the power supplied to the heater/cooler and to log the data from the sensors and the cameras. The Main Control Unit (MCU) is a PC equipped with serial interfaces, running LabVIEW® 2017. It connects via USB to the Power Control Unit, the DAU, the Thermocamera and the CMOS camera, both cameras are sampled at 1 Hz. The PCU is designed to drive the electric power to a Peltier Module as it features a true bipolar DC current source for cooling or heating.

The DAU acquires five temperatures and two heat flux sensors (max. error ± 0.1 W/cm^2). For the temperature measurements, 4-wire Platinum Resistance Pt-100 are coupled with a RTD-to-Digital converter (total maximum error on temperature measurements $\pm 0,2$ K). Three Pt-100 sensors are installed along the diagonal of the composite upper side (fig. 2), one on the Peltier cell and one for measuring the ambient temperature.

To measure the temperature map of the composite material during the experiment from the LWIR camera, a calibration process is performed, to consider the influence of the ZnSe window and of the environment. For every IR frame, the area around the Pt-100 is averaged and the resulting mean temperature is used as calibration reference, with a maximum error after calibration of ± 0.8 °C.

In order to perform experiments, the test cell is heated up at constant heat flux until the paraffin wax melts completely. During this period the temperature and the heat flux signals, as well as the greyscale and IR images, are recorded (acquisition rate 1Hz). After that, the Peltier module electric supply is inverted to cool down the test cell and solidify the paraffin as fast as possible and start another experiment. The acquisition lasts for the whole experiment duration. Depending on the experiment conditions, each test duration ranges from 40 to 60 minutes.
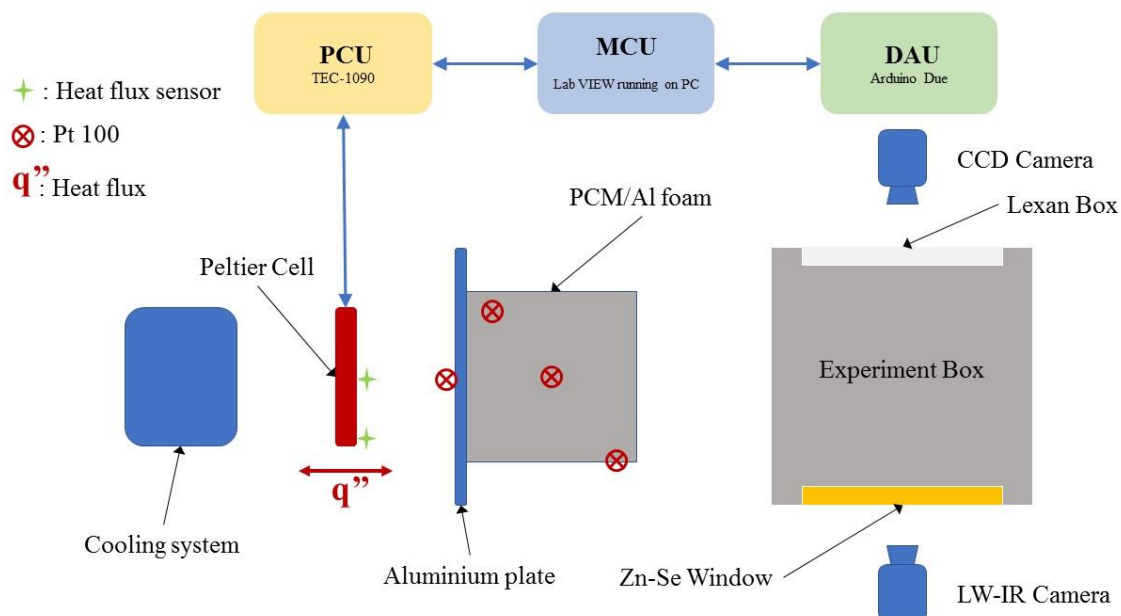

Figure 1. Experimental facility.

4. Results

Results are presented in terms of PCM melting fraction, that is represented by the function β introduced before. A comparison between numerical and experimental results for normal conditions, *i.e.* 1**g**, is presented in figure 2. Results are compared for three different times, in particular 240, 360 and 480 seconds, and a good agreement has been found. Slight differences might be attributed to the fact that in the experiments a small thermal dispersion to the environment might exists, causing the melting front to be slightly different between experiments and predictions. Besides, another reason could be some uncertainty related to heat flux, since in the model we assume that an average heat flux with respect to time is applied. This variation is assumed to be negligible in the model. In both experiments and predictions, it is shown that melting front develops with time because of applied heat. With references to numerical simulations, in the first time reported ($t = 240$ s), the front is almost parallel to the heat flux. This means that convection doesn't have a primary role for this times and conduction is the dominant heat transfer mechanism. The more the time, the more the front becomes less parallel. This because convection starts to become important since temperatures are rising up, thus buoyancy forces become higher. This will be explained in detail later.

The effects of hypergravity on melting fraction is presented in figure 3, for three different gravity levels, i. e. 1**g**, 5**g** and 10**g**, and $t = 240$, 360 and 480 s. It is shown that melting front develops faster with higher gravity levels because of the increase of buoyancy forces, especially in the top part of the computational domain because convection tends to drive the liquid PCM in the upper part. This faster developing increases for higher times because convection becomes generally important, as previously shown in figure 2.
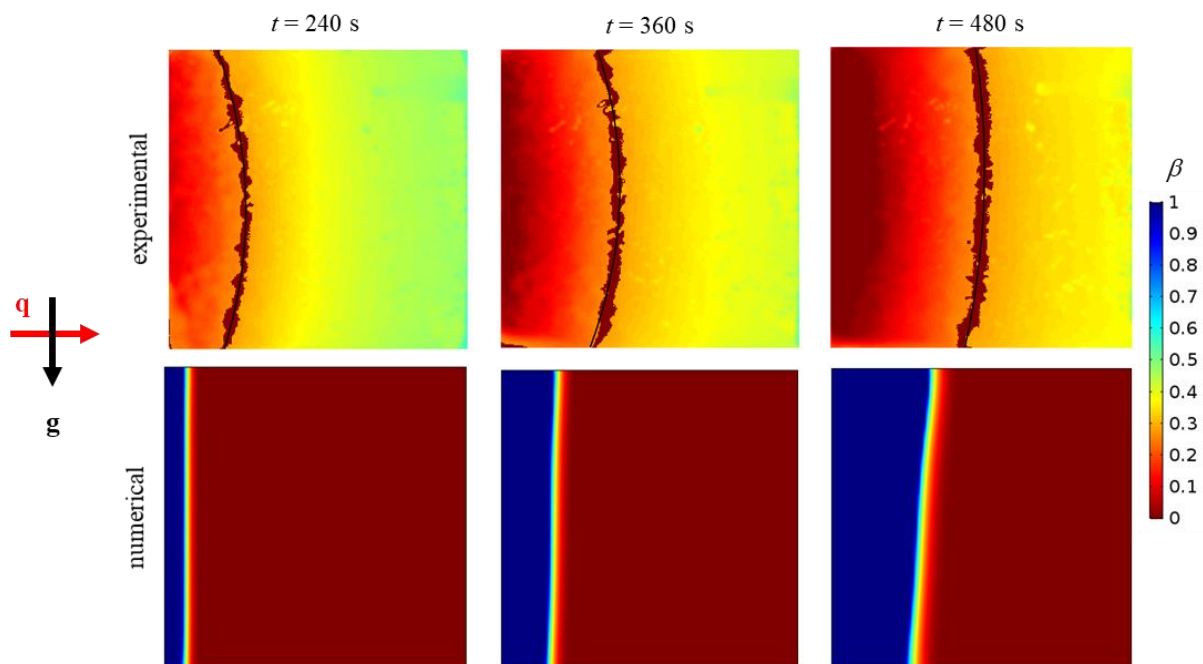

Figure 2. Comparisons between experimental and numerical results in terms of PCM melting fraction β for 40 PPI and $|\mathbf{q}| = 11520$ W/m^2 with orthogonal heat flux and gravity vectors.
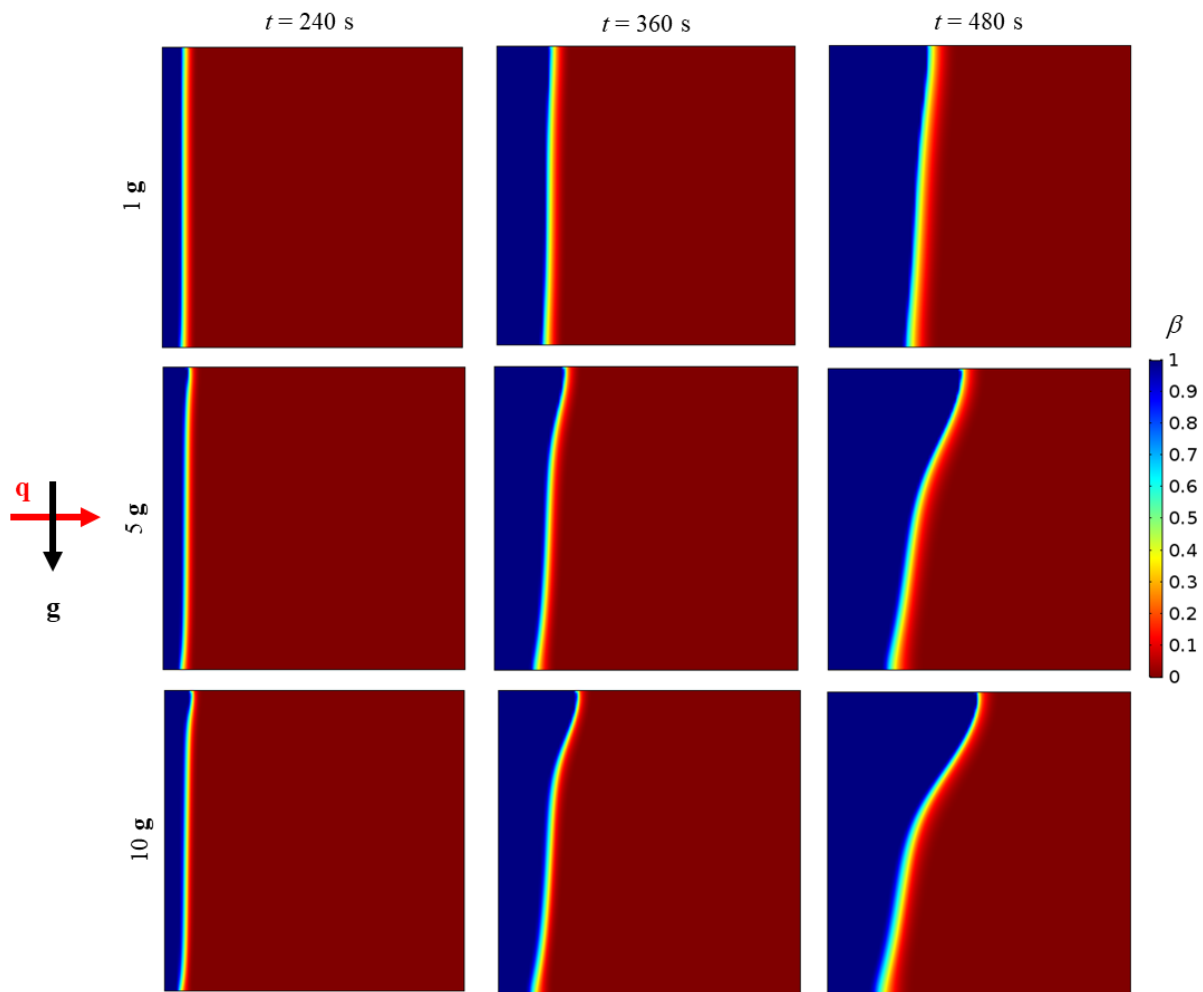
Figure 3. Effects of hypergravity on PCM melting fraction β for 40 PPI and $|\mathbf{q}| = 11520$ W/m^2 with orthogonal heat flux and gravity vectors.

5. Conclusions

The effects of hypergravity on heat transfer in a phase change material coupled with a metal foam has been numerically investigated. The mathematical model has been developed with references to the porous media theory, while phase change is modelled with the apparent heat capacity method. Under a uniform heat flux boundary condition, transient-state governing equations are solved with the finite element method for different gravity levels. In-house experiments have been also carried out in order to validate the model for normal gravity conditions, and a good agreement between simulations and experiments has been found in terms of melting fraction. With references to simulations performed with different gravity levels, it has been found that convection becomes very important for higher gravity accelerations, and the melting front becomes very variable along the gravity vector coordinate.

References

[1]   Dincer I and Rosen M A 2002 *Thermal energy storage systems and applications* (John Wiley & Sons)

[2]   Sharma A, Tyagi V V, Chen C R and Buddhi D 2009 *Renew. Sust. Energ. Rev.* **13(2)** 318-45

[3]   Iasiello M, Braimakis K, Andreozzi A and Karellas S 2017 *J. Phys. Conference Series* **796(1)** 012042 IOP Publishing

[4]   Qureshi Z A, Ali H M and Khushnood S 2018 *Int. J. Heat Mass Transfer* **127** 838-56

[5]   Wang C, Lin T, Li N and Zheng H 2016 *Renewable energy* **96** 960-5

[6]   Mancin S, Diani A, Doretti L, Hooman K and Rossetto L 2015 *Int. J. Thermal Sciences* **90** 79-89

[7]   Lafdi K, Mesalhy O and Shaikh S 2007 *J. Appl. Phys.* **102(8)** 083549.

[8]   Whitaker S and Quintard M 2005 Coupled, nonlinear mass transfer and heterogeneous reaction in porous media *Handbook of Porous Media* ed K Vafai (Boca Raton: Crc Press) chapter 1 pp 21-56

[9]   Feng S, Shi M, Li Y and Lu T J 2015 *Int. J. Heat Mass Transfer* **90** 838-47.

[10]   Zhu F, Zhang C and Gong X 2016 *Appl. Therm. Eng.* **109** 373-83.

[11]   Di Giorgio P, Iasiello M, Viglione A, Mameli M, Filippeschi S, Di Marco P, Andreozzi A and Bianco N 2017 *J. Phys. Conference Series* **796(1)** 012032 IOP Publishing

[12]   Tian Y and Zhao C Y 2011 *Energy* **36(9)** 5539-46

[13]   Li W. Q, Qu Z G, He Y L and Tao W Q 2012 *Appl. Thermal Eng.* **37** 1-9

[14]   Nannipieri P, Anichini M, Barsocchi L, Becatti G, Buoni L, Celi F, ..., and Guardati P *J. Phys. Conference Series* **796(1)** 012044 IOP Publishing

[15]   Calmidi 1998 *Transport Phenomena in High Porosity Metal Foams* (PHD Thesis - University of Colorado U.S.A.)

[16]   Churchill S W and Chu H H 1975 *Int. J. Heat Mass Transfer* **18(9)** 1049-53

[17]   Georgiadis J G and Catton I 1988 *Int. J. Heat Mass Transfer* **31(5)**, 1081-91.

[18]   Iasiello M, Bianco N, Chiu W K S and Naso V 2019 *Int. J. Thermal Sciences* **137** 399-409.

[19]   Kheirabadi A C and Groulx D 2015 *Proc. of CHT-15 (Piscataway)* (Begell House, Inc.) CHT-15-077.

[20]   Andreozzi A, Bianco N, Iasiello M and Naso V 2019 Natural convection in a vertical channel with open-cell foams *Proceedings of the 37th UIT Heat Transfer Conference*.